ACS APPLIED MATERIALS & INTERFACES

Research Article

www.acsami.org

Tunable Ternary (N, P, B)-Doped Porous Nanocarbons and Their Catalytic Properties for Oxygen Reduction Reaction

Shunyan Zhao, Juan Liu, Chuanxi Li, Wenbing Ji, Manman Yang, Hui Huang, Yang Liu,* and Zhenhui Kang*

Institute of Functional Nano & Soft Materials (FUNSOM), Soochow University, Suzhou 215123, China

Supporting Information

ABSTRACT: Heteroatom (N, P, and B)-codoped nanocarbons (NPBC) with nanoporous morphology are fabricated via a facile one-step pyrolysis method and exhibit good electrocatalytic activity, durability, and selectivity for the oxygen reduction reaction (ORR) in alkaline media. The ORR activity of NPBC is better than single- (nitrogen-doped carbon (NC)) or dual-doped (nitrogen and phosphorus codoped carbon (NPC) or nitrogen and boron codoped carbon (NBC)) catalysts in terms of onset potential and current density. This synthetic approach is efficient and suitable for large-scale fabrication of metal-free carbon-based catalysts.

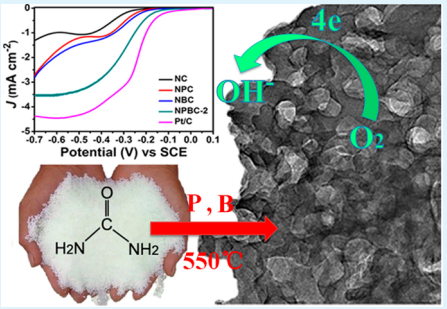

KEYWORDS: *nitrogen, phosphorus, boron, ternary-doped, nanocarbon, oxygen reduction reaction*

1. INTRODUCTION

The energy crisis makes the exploration of efficient catalysts for cathodic oxygen reduction reaction (ORR) in fuel cells an urgent challenge in present material chemistry.[1,2] Platinum-based catalysts have been identified as the most effective catalysts for ORR.[3,4] However, the sluggish kinetics, limited reserves, high cost, and poor durability of platinum hinder the large-scale commercialization of platinum-based catalysts. To date, extensive research efforts have been directed toward the search for alternative catalysts based on doping materials, such as Co or Fe-based catalysts,[5−7] and metal-free materials, such as carbon-based materials (carbon nanotubes (CNTs),[8] graphene,[9,10] mesoporous graphitic arrays,[11] mesoporous carbon,[12] and carbon nitride[13−15]). Carbon-based materials doped with nonmetal heteroatoms (B, N, S, P, and I) have been considered as promising candidates for replacing platinum-based catalysts due to their pronounced electrocatalytic activities, long-term stability, excellent tolerance against crossover effects, and relatively low costs.[16,17]

For carbon-based catalysts, numerous efforts have been devoted to N-doped carbon, a universal heterogeneous carbon-based catalyst for ORR.[18−20] The additional introduction of other heteroatoms, such as B, P, or S, further alters the properties of the carbon and enhances its catalytic activity. Most previous studies focused on binary-doped carbon materials, such as B−N, P−N, and S−N,[21−23] which performed better than single N-doped materials. For example, Liu et al. reported boron and nitrogen codoped nanodiamond in which the high ORR activity was attributed to the synergetic effect of codopants boron and nitrogen.[24] Xu et al. developed sulfur and nitrogen dual-doped ordered mesoporous carbon, which performed a positive onset voltage, but the template etching method was inconvenient and the intermediate Fe catalyst may affect the ORR performance.[25] Besides the work focused on the binary doping of heteroatoms into the carbon structure, the ternary-doped carbon material for ORR is highly desired and still remains a big challenge.

Herein, we reported the controllable fabrication of nitrogen, phosphorus, and boron codoped carbon (NPBC) with porous nanostructures by a facile pyrolysis method. It was demonstrated that the tunable ternary (N, P, B)-doping of NPBC could be realized by altering the ratio of phosphoric acid and boracic acid in the raw materials. The NPBC, as metal-free catalysts, exhibited favorable activity for ORR in alkaline medium compared with nitrogen-doped carbon (NC), nitrogen and phosphorus codoped carbon (NPC), and nitrogen and boron codoped carbon (NBC).

2. EXPERIMENTAL SECTION

All the chemicals used in this work were used as obtained without further purification and commercially available unless otherwise stated.

2.1. Synthesis of Nitrogen, Phosphorus, and Boron Codoped Carbon (NPBC). In a typical synthesis, 10 g of urea, 3 mL of 0.1 M phosphoric acid, and 7 mL of 0.1 M boracic acid were put into a crucible with a cover, heated to 100 °C from room temperature rapidly, then heated to 550 °C (450 or 600 °C) with a heating rate of 5 °C/min, and finally maintained at the temperature for 3 h in a muffle furnace. Ultimately, yellow sample was obtained after spontaneous cooling and was designated as NPBC-2. We altered the proportion of phosphoric acid and boracic acid to obtain NPBC with different phosphorus and boron contents. Detailed precursor compositions of

Received: September 13, 2014
Accepted: November 25, 2014
Published: November 25, 2014

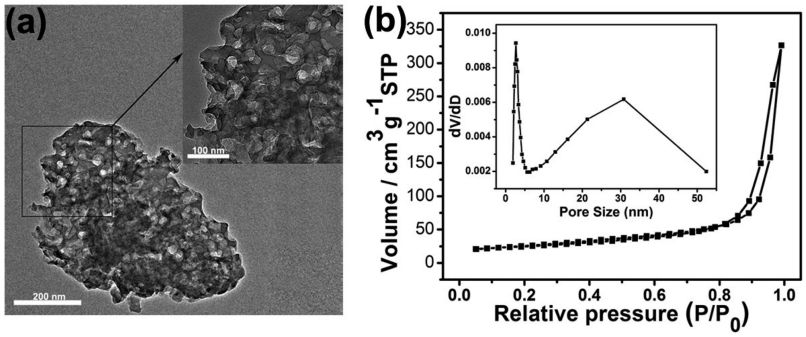

Figure 1. (a) Low-magnification and (inset) high-magnification TEM images of NPBC-2. (b) N_2 adsorption−desorption isotherms for NPBC-2 and (inset) the corresponding BJH pore-size distribution curve.

synthesized samples are described in Table S1 (Supporting Information). All as-prepared products were kept intact and collected before characterization and further use.

2.2. Synthesis of Nitrogen-Doped Carbon (NC), Nitrogen and Phosphorus Codoped Carbon (NPC), or Nitrogen and Boron Codoped Carbon (NBC). All samples for controlled trials were prepared by the similar steps of NPBC-2 synthesis with different precursors. NC was obtained by direct pyrolysis of the urea. NPC was prepared by heating the mixture of urea and phosphoric acid. NBC was synthesized by heating the mixture of urea and boracic acid. The heating procedures were the same as above. Detailed precursor compositions of synthesized samples are described in Table S1, Supporting Information. All as-prepared products were kept intact and collected before characterization and further use.

2.3. Structure and Morphology Characterizations. An FEI-quanta 200 scanning electron microscope with acceleration voltage of 20 kV were taken to measure scanning electron microscopy (SEM) images and energy dispersive X-ray analysis (EDX) spectroscopy. The compositions of obtained samples were measured by EDX. Transmission electron microscope (TEM) images are obtained with a FEI-Tecnai F20 (200 kV). The usual TEM products were prepared through dropping the solution onto a copper grid with polyvinyl formal support film and dried in air. The structure of the samples was characterized by powder X-ray diffraction (XRD) by using an X'Pert-ProMPD (Holand) D/max-γAX-ray diffractometer with Cu Kα radiation (λ = 0.154178 nm). X-ray photoelectron spectroscopy (XPS) was performed with a KRATOS Axis Ultra-DLD X-ray photoelectron spectrometer with a monochromatised Al Kα X-ray ($h\nu$ = 1486.6 eV). UV−vis absorption was recorded on a Lambda 750 (PerkinElmer) spectrophotometer in the wavelength range of 200−1000 nm. Fourier transform infrared (FT-IR) spectroscopy (Nicolet 6700 FT-IR spectrophotometer) was employed to characterize the microstructure of as-synthesized products with a scanning range of 4000−400 cm^{-1} at room temperature.

2.4. Electrochemical Measurements. The electrocatalytic characterization was performed by cyclic voltammograms (CV), linear sweep voltammograms (LSV) and chronoamperometric measurements in a standard three-electrode electrochemical cell, which was connected to an electrochemical workstation (CHI 920C, CH Instrument, Shanghai) coupled with a rotating disk electrode (RDE) system (ATA-1B, Jiangfen Electroanalytical Instrument Co., Ltd., China) and a rotating ring-disk electrode (RRDE) system (HP-1A, Jiangfen Electroanalytical Instrument Co. Ltd., China). A platinum wire and a saturated calomel electrode (SCE) were used as the counter electrode and the reference electrode, respectively. To prepare the working electrode, 5 μL of catalyst solution (1.5 mg·mL^{-1}) was dropped onto the glassy carbon electrode (GCE, 0.0707 cm^2), leading to the catalyst loading ~0.1 mg·cm^{-2}, followed by coating with 5 μL of Nafion solution (0.5 wt %) and dried at room temperature.

The CV measurements were performed in N_2- and O_2-saturated 0.1 M KOH solutions with a scan rate of 50 mV·s^{-1}. The RDE measurements were conducted in the O_2-saturated 0.1 M KOH solution at rotation speeds ranging from 300 to 1600 rpm and with the scan rate of 10 mV·s^{-1}. The RRDE measurements were performed at a rotation speed of 1600 rpm with a scan rate of 10 mV·s^{-1} and the ring potential was constant at 0.5 V. The chronoamperometric measurements were performed at −0.3 V for 10 h. The electron transfer numbers and the kinetic current density can be calculated from the slope and intercept of the Koutecky−Levich plots, respectively:[6]

$$\frac{1}{J} = \frac{1}{J_k} + \frac{1}{Bw^{0.5}} \quad (1)$$

$$B = 0.2nFv^{-1/6}C_{O_2}D_{O_2}^{2/3} \quad (2)$$

where J is the measured current density, J_k is the kinetic current density, and w is the revolutions per minute of the disk. The constant 0.2 is adopted when the rotation speed is expressed in terms of rpm; n is the overall number of electrons transferred in oxygen reduction; F is the Faraday constant (F = 96485 C·mol^{-1}), C_{O_2} is the bulk concentration of O_2 (C_{O_2} = 1.2 × 10^{-6} mol·cm^{-3}), ν is the kinematic viscosity of the 0.1 M KOH solution (ν = 0.011 cm^2·s^{-1}), and D_{O_2} is the diffusion coefficient of O_2 in 0.1 M KOH solution (D_{O_2} = 1.9 × 10^{-5} cm^2·s^{-1}).

3. RESULTS AND DISCUSSION

In this study, the nitrogen-doped carbon (NC), nitrogen and phosphorus codoped carbon (NPC), nitrogen and boron codoped carbon (NBC) and nitrogen, phosphorus, and boron codoped carbon (NPBC) with varying boron and phosphorus contents have been synthesized to investigate the influence of heteroatom doping on carbon materials toward ORR. The original and final compositions of obtained samples were shown in Tables S1 and S2 (Supporting Information), respectively. The relative surface concentrations of NPBC-2, NC, NBC and NPC were characterized by XPS (Table S3, Supporting Information).

Here, a series of detailed discussion about morphology and structure of the products were carried out based on typical one of NPBC-2. The SEM images (Figure S1a,b, Supporting Information) and the TEM images (Figure S1c,d, Supporting Information) suggested that NPBC-2 was film-like carbon with porous structure. A high-magnification TEM image of NPBC-2 (Figure 1a, inset) further confirmed the bubble-like and irregular morphology. To further demonstrate its porous structure, we carried out the nitrogen BET (Brunauer−Emmet−Teller) adsorption measurements of NPBC-2. As shown in Figure 1b, the BET specific surface area of NPBC-2 was 89.5 m^2·g^{-1}, which was about 2 times as high as that of NC catalysts (44.9 m^2·g^{-1}; Figure S3, Supporting Information). The pore size distribution was presented in the inset in Figure 1b. An apparent pore size distribution of NPBC-2 could be

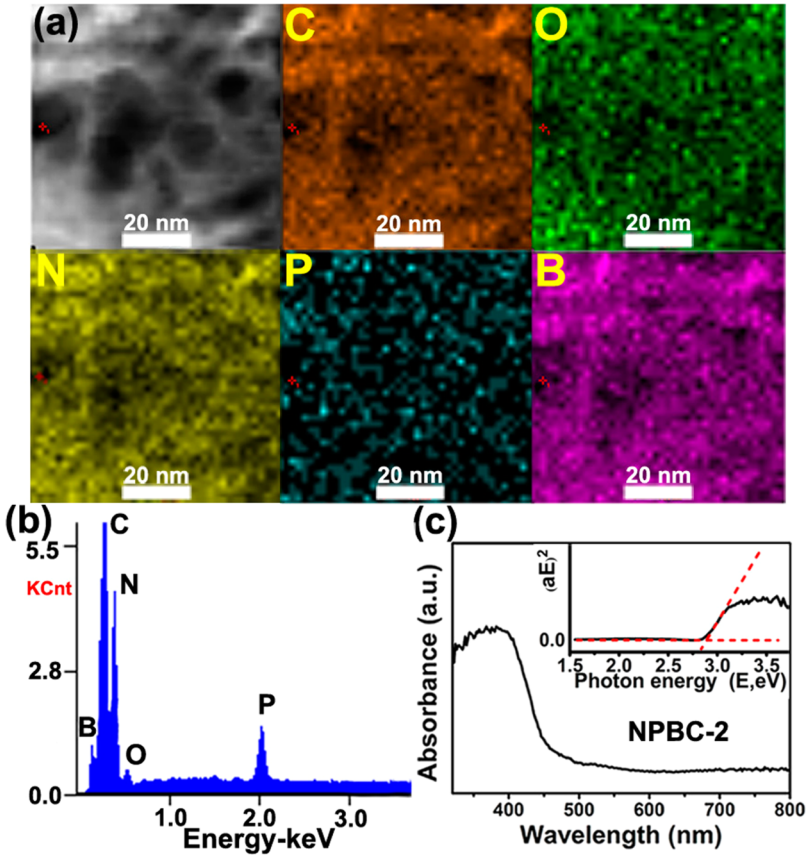

Figure 2. (a) STEM image and the corresponding elemental mapping images of NPBC-2. (b) EDS profile of NPBC-2. (c) Optical absorption spectra of NPBC-2 and (inset) plots of $(aE)^2$ against the photon energy.

observed, which mainly distributed at about 2.7 nm, and had a broad peak at 10−50 nm. Thus, the doping of phosphorus and boron element facilitated the formation of large surface area during the pyrolysis process.

As shown in Figure 2a, the STEM and the corresponding elemental mapping images revealed that the NPBC-2 sample consisted of C, N, O, P, and B, and the P and B elements in the carbon structure were distributed evenly. This suggested that nitrogen, phosphorus and boron were all doped in the carbon successfully. The EDS profile of the NPBC-2 also confirmed the presence of nitrogen, phosphorus, and boron (Figure 2b). Figure 2c showed the absorbance spectra of NPBC-2 with an absorption onset at about 500 nm. The square of the absorption energy (aE, where E is the photo energy and a is the absorbance) against E could decide the energies of the direct gap transitions.[26] From approximate linear extrapolation, the inset in Figure 2c gave apparent energies of 2.86 eV of the direct transition for the NPBC-2 specimen, 2.82 eV for NC, 2.78 eV for NPC, and 2.90 eV for NBC (Figure S2, Supporting Information).

Figure 3a showed the XRD patterns of NPBC-2, NBC, NPC and NC. The distinct (002) peak at 27.43° in the black line could be attributed to the interlayer spacing of 0.326 nm and the (100) diffraction peak at 12.76° corresponded to the in-plane ordering of tri-*s*-triazine units.[27,28] As shown by the green line for NPBC-2 (Figure 3a), the XRD pattern showed a significant decrease of intensity and the peak corresponding to (002) shifted to 26.92° after N, P, and B codoping into the carbon structure. As shown in Figure 3b, the FT-IR spectra showed that after the doping of boron and phosphorus, the

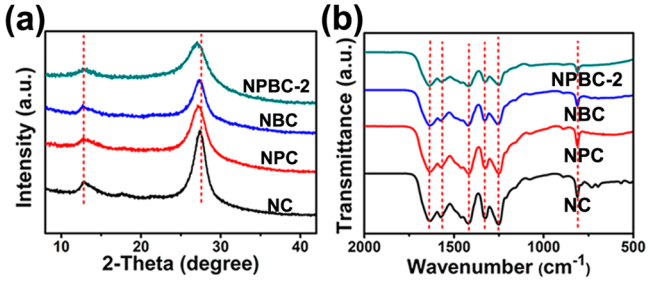

Figure 3. (a) XRD patterns and (b) FT-IR spectra of NC, NPC, NBC, and NPBC-2.

carbon nitride network remained nearly invariable. It could be clearly seen that the characteristic peaks of the breathing vibration (808.5 cm^{-1}) and the stretching vibrations of the tri-*s*-triazine units (1250−1650 cm^{-1}) appeared on the FT-IR spectra of all samples, and the peak positions were nearly the same, indicating that the framework structures and functional groups were analogous to each other.

X-ray photoelectron spectroscopy (XPS) measurements were measured to analyze the chemical environment of the N-, P-, B-doped carbon structures. In Figure 4a, the full XPS survey spectrum showed the C 1s, N 1s, and O 1s peaks of the nitrogen-doped carbon (NC). Compared with the full XPS survey spectrum of NC, the existence of phosphorus and boron in Figure 4b suggested that NPBC-2 consisted of C, N, O, P and B. The presence of N, P, and B elements in the EDS spectrum (Figure 2b) confirmed the XPS analysis. The high-resolution XPS spectra of C 1s, N 1s, B 1s, and P 2p of the

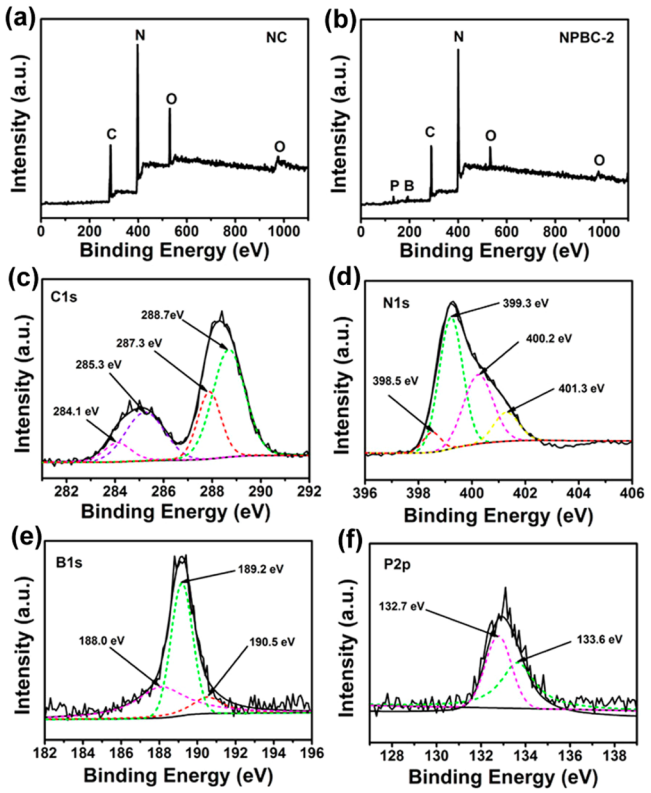

Figure 4. XPS survey spectra of (a) NC and (b) NPBC-2; (c) C 1s, (d) N 1s, (e) B 1s, and (f) P 2p XPS signals for NPBC-2.

obtained NPBC-2 sample are shown in Figure 4. The C 1s peak (Figure 4c) could be divided into four components located at 284.1, 285.3, 287.3, and 288.7 eV, respectively, which could be ascribed to C−C, C−P, C−O, and C−N bonding, respectively.[29−31] The existence of the C−P bonding confirmed that phosphorus was successfully doped in NPBC-2. Another peak at 287.3 eV corresponding to C−O stemmed from the urea precursor, and the peak at 288.7 eV was regarded as originating from C, which was bonded with three N neighbors. The high-resolution N 1s spectrum of nitrogen-doped carbon (NC) displayed three binding energies and they could be ascribed to C−N−C (399.0 eV), N−$(C)_3$ (399.9 eV), and N−N groups (401.2 eV), respectively (Figure S4, Supporting Information).[24,28,32] These representative signals also appeared in N 1s spectrum of NPBC-2 (Figure 4d), indicating that the framework of NC remained unchanged with the doping of boron and phosphorus. Moreover, the peak at 398.5 eV indicated the formation of pyridinic−N, which was associated with N−B bond.[24] According to the B 1s spectra in Figure 4e, the peak at 188.0 eV was assigned to B−C bonding,[32] while the peak at 189.2 eV was related to the B−N−C bonding.[24,33,34] The peak at 190.5 eV was related to the B−N bond.[24] In Figure 4f, the peaks at 132.7 and 133.6 eV could be attributed to P−C and P−O bonding, respectively.[30,35,36] The existence of the P−C covalent bonding confirmed that phosphorus had been successfully doped into the NPBC-2. The presence of P−O bonding implied the doped P atoms might be partially oxidized in the pyrolysis process.[30]

The CV and RDE curves were performanced to measure the activities of NPBC-2 for cathodic ORR. Meanwhile, we also synthesized the NC, NPC, and NBC and tested their ORR activities. First, the ORR activity of NC, NPC, NBC, and NPBC-2 was examined by CV in N_2-saturated and O_2-saturated 0.1 M KOH solutions. In Figure 5a, the obvious reduction

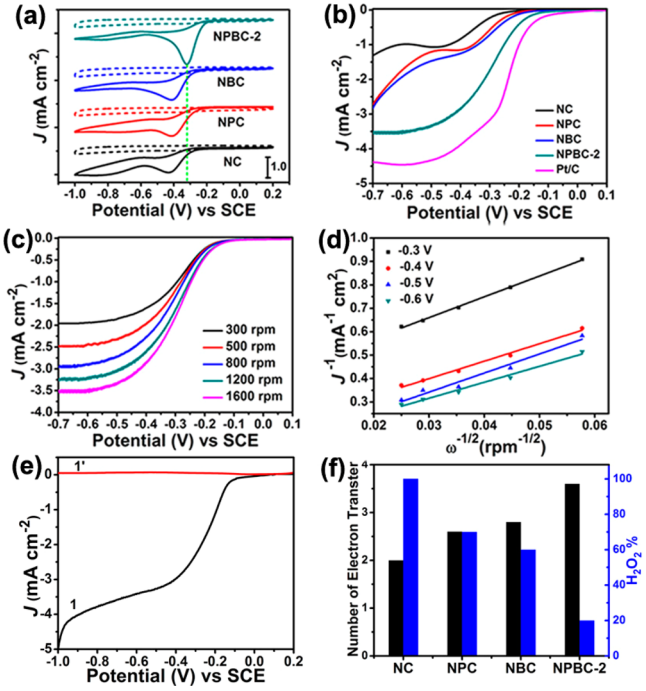

Figure 5. (a) CV curves of NC, NPC, NBC, and NPBC-2 in (solid line) O_2-saturated or (dashed line) N_2-saturated 0.1 M KOH solutions with a scan rate of 50 mV·s^{-1}. (b) LSVs of the NC, NPC, NBC, NPBC-2, and commercial Pt/C in an O_2-saturated 0.1 M KOH solution at a rotation rate of 1600 rpm and a scanning rate of 10 mV·s^{-1}. (c) RDE voltammograms of the NPBC-2 in an O_2-saturated 0.1 M KOH solution at 10 mV·s^{-1} and various rotation speeds. (d) Koutecky−Levich plots of j^{-1} versus $\omega^{-1/2}$ of the NPBC-2 at potentials of −0.3, −0.4, −0.5, and −0.6 V. (e) Rotating ring-disk electrode (RRDE) LSV curves for NPBC-2 with a rotation rate of 1600 rpm in an O_2 saturated 0.1 M KOH solution at 10 mV·s^{-1}; (1) disk current density and (1′) ring current density obtained from the NPBC-2 catalyst. (f) The calculated percentage of H_2O_2 and electron transfer numbers (n) of various samples.

peaks occurred in the O_2-saturated 0.1 M KOH solution using all the four catalysts, while the featureless peaks were observed within the same potential range in the N_2-saturated 0.1 M KOH solution. The ORR peak potential was −0.32 V for NPBC-2, which was ∼0.09 V more positive than that of NPC and 0.08 V more positive than that of NBC. This value was much more positive than that of NC (−0.44 V). Commercial Pt/C was also measured. For the NC, NPC, NBC, NPBC-2, and Pt/C, respectively, the onset potentials were −0.22, −0.17, −0.16, −0.11, and −0.06 V, respectively (Figure 5b). Remarkably, the NPBC-2 electrode exhibited more positive onset potential and larger current than those of NC, NPC, and NBC. Clearly, the positive shift of onset potential and enhancement of reduction current on NPBC-2 electrode indicated that NPBC-2 possessed of much higher electrocatalytic activity toward ORR than NC, NPC, and NBC. RDE measurements were performed with varying rotation speeds from 300 to 1600 rpm (Figure 5c). The oxygen reduction current density increased with increasing rotation rate. The Koutecky−Levich plots at different electrode potentials derived from Figure 5c displayed good linearity (Figure 5d). The electron transfer number (n) of NPBC-2 was calculated to be about 3.6 at the potential range from −0.3 to

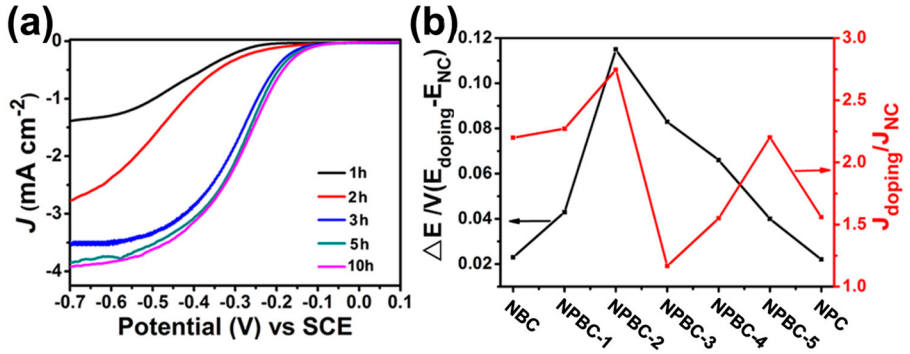

Figure 6. (a) LSV curves of ORR on the NPBC-2 samples prepared under different heating time in an O_2-saturated 0.1 M KOH solution with a scan rate of 10 mV·s^{-1} at a rotation rate of 1600 rpm. (b) The plot of (black line) peak potential and (red line) peak current density of ORR on NPBC electrodes normalized to NC.

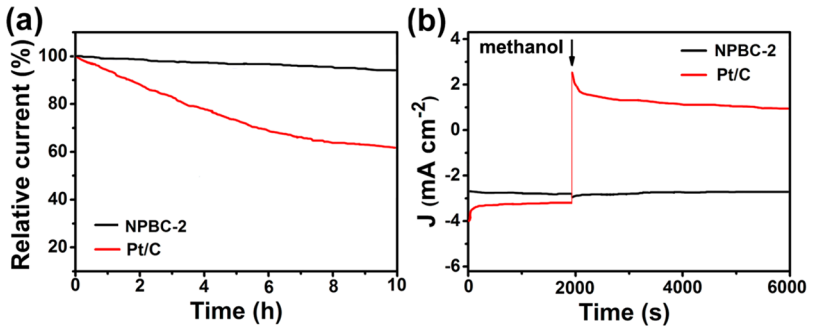

Figure 7. (a) The current−time (i−t) curves of NPBC-2 and 20% Pt/C catalysts at −0.3 V (vs SCE) in an O_2-saturated 0.1 M KOH solution for 10 h. (b) Chronoamperometric responses of NPBC-2 and 20% Pt/C catalysts at −0.3 V in an O_2-saturated 0.1 M KOH solution without methanol (0−2000 s) and with adding methanol (2000−6000 s). The arrow represents the addition of methanol.

−0.6 V according to the slopes of Koutecky−Levich plots, indicating a more efficient four-electron pathway during the ORR process. RRDE was measured to further confirm the electron transfer number (n), a significant kinetic parameter to investigate the ORR efficiency of NPBC-2 (Figure 5e).

The electron transfer number (n) could be calculated by the following equation:[37]

$$n = 4I_d/(I_d + I_r/N) \quad (3)$$

$$H_2O_2\ (\%) = 100 \times (4 - n)/2 \quad (4)$$

where I_d is the disk current density, I_r is the ring current density and N = 0.24 is the current collection efficiency. The electron transfer number (n) of the NPBC-2 catalyst was calculated to be 3.58, which was consistent with the result calculated from the slopes of the Koutecky−Levich plots, indicating a nearly 4e$^-$ pathway. Figure S5a,c,e (Supporting Information) showed the RDE curves of NC, NPC, and NBC electrodes at different rotation speeds, respectively. Figure S5b,d,f (Supporting Information) showed the corresponding Koutecky−Levich plots of J^{-1} versus $\omega^{-1/2}$ of NC, NPC and NBC electrodes, respectively. The electron transfer numbers were estimated to be about 2.0 (NC), 2.6 (NPC), and 2.8 (NBC), respectively, agreeing well with the results from the RRDE curves (Figure 5f; Figure S6, Supporting Information), which explained the ORR efficiency catalyzed by NC (or NPC, NBC) was below that by NPBC-2. As shown in Figure 5f, the percentages of H_2O_2 in NC, NPC, NBC and NPBC-2 were about 100, 70, 60, and 20%, respectively. Thereby, we could suggest the NPBC-2 catalyst showed better ORR efficiency from the nearly 4e$^-$ dominated process.

The electrocatalytic activity of NPBC-2 at various treatment temperatures were studied by LSV measurements. Figure S7 (Supporting Information) revealed that NPBC-2 (550 °C) showed the best performance. Then, we investigated the influence of heat-treatment time on the ORR activity of NPBC-2. The samples were maintained at 550 °C for 1, 2, 3, 5, and 10 h, respectively, and are denoted as NPBC-2 (1 h), NPBC-2 (2 h), NPBC-2 (3 h), NPBC-2 (5 h) and NPBC-2 (10 h), respectively. As shown in Figure 6a, NPBC-2 (1 h) exhibited the lowest ORR performance of all, while NPBC-2 (2 h) revealed better performance compared with NPBC-2 (1 h). The NPBC-2 (3 h) displayed a significantly enhanced current density and much more positive onset potential than NPBC-2 (2 h) and NPBC-2 (1 h). NPBC-2 (5 h) performed with a tiny improvement of ORR activity over that of NPBC-2 (3 h), and the catalytic activity of NPBC-2 (10 h) showed almost no change compared with NPBC-2 (5 h) in terms of the current density and onset potential. The obvious enhancement of NPBC-2 (3, 5, and 10 h) may be attributed to the influence of heating time on the structure and specific surface area of catalysts. According to the corresponding BET results of different catalysts in Table S4 (Supporting Information), the heat-treatment time changed the specific surface area and pore size of the catalysts. When the heating time exceeded 3 h, the specific surface area of the catalysts increased scarcely. Therefore, it could be concluded that the increased specific surface area would enhance the ORR activity of the catalysts.

To further investigate the influence of dopants on the ORR performance, five NPBC samples with different contents of phosphorus and boron were prepared by altering the proportion of phosphoric acid and boracic acid in raw materials

(Table S1, Supporting Information). The peak potential and peak current density of NPBC electrodes are shown in Figure 6b. The NPBC catalysts with different contents of phosphorus and boron showed various ORR activities. Here, the peak potential and peak current density of NC were used as the references. The NPBC-2 (the initial molar ratio of P/B was 3:7) exhibited the best performance, that is, the peak potential (−0.32 V) was more positive than that of NC (−0.44 V) and the peak current density was 2.75 times as large as that of NC. Interestingly, the peak current density of NPBC-3 (the initial molar ratio of P/B was 5:5) was close to that of NC. By controlling the initial molar ratio of P/B, the peak potential and peak current of the NPBC nanocatalysts could be remarkably promoted. In the series of samples, the N dopant remained almost unchanged. The results indicated that the nitrogen, phosphorus, and boron in carbon material with appropriate doping amounts synergistically improved the ORR activity.

Another vital consideration about electrocatalysts is their stability in fuel cells. To evaluate the stability of obtained catalysts, we conducted continuous chronoamperometric measurements of 10 h for NPBC-2, NPC, and NBC toward ORR at −0.3 V in an O_2-saturated 0.1 M KOH solution compared with commercial Pt/C catalyst. As shown in Figure 7a and Figure S8 (Supporting Information), NPBC-2, NPC, and NBC all exhibited tardy attenuation, especially the NPBC-2, which showed a high relative current of 95% over 10 h, but the commercial Pt/C catalyst merely kept 58% of the original current within the same time. The result demonstrated that NPBC-2 held better stability performance compared with that for Pt/C toward ORR in an alkaline medium. To examine possible crossover effects, we measured the electrocatalytic selectivity of NPBC-2, NPC, NBC, and 20% Pt/C against the electrooxidation of methanol in an O_2-saturated 0.1 M KOH solution by adding 3 mL of methanol at 2000 s. The ORR current of commercial Pt/C catalyst exhibited a sudden change after the methanol injection owing to the electrochemical oxidization of methanol (Figure 7b). However, the NPBC-2 remained almost unchanged under the same condition. This may be ascribed to the excellent stability of the ternary-doped carbon material as well as the synergetic effect of N, P, and B among the carbon framework. NPBC-2 exhibited high selectivity toward ORR with excellent performance in avoiding crossover effects, which had an advantage over the 20% Pt/C catalyst.

These results demonstrated that the doping of nitrogen, phosphorus and boron into carbon material had an important influence on the peak potential, electron transfer number, onset potential and current density. Two possible important reasons for the enhanced ORR activity were as follows. On one hand, the synchronous introduction of nitrogen, phosphorus, and boron led to the highly intricate surface structures of the as-prepared carbon materials. The film-shaped catalysts with porous structure and large special surface area may provide favorable reaction spaces and enough active catalytic sites for oxygen reduction, leading to their significantly enhanced ORR activity.[22,38−40] Additionally, the synergistic effect of heteroatoms (N, P, and B) among carbon framework may be a crucial factor influencing the electrochemical performance of NPBC. The doping of nonmetal heteroatoms in the sp^2 carbon framework could break the electroneutrality of carbon and generate active sites for O_2 adsorption, no matter if the heteroatom electronegativity is higher or lower than the carbon value of 2.55 (N: 3.04, B: 2.04, P: 2.19).[41−43] The ternary doping of N, P, and B may introduce asymmetrical spin and charge density, inducing a larger number of active C atoms.[44] The underlying synergistic effect among heteroatoms may result from the enhanced disturbance to the uniform electronic structure of the carbon surfaces.[41] Compared to previous research (Table S5, Supporting Information), our present work has made a breakthrough for the low-cost, facile fabrication of heteroatom (N, P, and B) codoped nanocarbon (NPBC) composite with highly efficient ORR activity. In addition, we have analyzed the influence of different contents of P and B on the catalytic ORR performance of NPBC in detail and found an interesting trend.

4. CONCLUSIONS

In summary, we synthesized the N, P, and B codoped carbon by an effective, simple, and easily reproducible method. As a metal-free catalyst, the resulting NPBC sample showed good electrocatalytic activity, long-term stability, and superb resistance to crossover effects for oxygen reduction reaction in alkaline media. The synergetic effect of N, P, and B among the carbon framework by chemical doping strategy promoted the formation of active sites for ORR. We have also investigated the influence of different contents of P and B on catalytic ORR performance of NPBC and found that NPBC-2 outperformed the catalysts with other ratios of P and B. Such novel and high-efficiency ternary-doped carbon-based catalyst could give a promising substitute for commercial Pt/C in the future.

■ ASSOCIATED CONTENT

Ⓢ Supporting Information

Initial compositions of the prepared samples; elemental compositions of the samples after doping; electrochemically active data for ORR of previous reports and our work; additional TEM and SEM images; physicochemical properties of NPBC-2; additional EDS, XPS, and optical absorption spectra; N_2 adsorption−desorption properties of NC, NPC, and NBC samples; RDE voltammograms; and the current−time (i−t) chronoamperometric response of the NC, NPC, and NBC. This material is available free of charge via the Internet at http://pubs.acs.org.

■ AUTHOR INFORMATION

Corresponding Authors

* E-mail: zhkang@suda.edu.cn.
* E-mail: yangl@suda.edu.cn.

Author Contributions

The manuscript was written through contributions of all authors. All authors have given approval to the final version of the manuscript.

Notes

The authors declare no competing financial interest.

■ ACKNOWLEDGMENTS

This work is supported by Jiangsu Key Laboratory for Carbon-based Functional Materials and Devices, and Collaborative Innovation Center of Suzhou Nano Science and Technology, the National Natural Science Foundation of China (51422207, 51132006, 21471106), a Suzhou Planning Project of Science and Technology (ZXG2012028), a project funded by the Priority Academic Program Development of Jiangsu Higher Education Institutions (PAPD), the National Basic Research Program of China (973 Program) (2012CB825803,

2013CB932702), and the Specialized Research Fund for the Doctoral Program of Higher Education (20123201110018),

REFERENCES

(1) Snyder, J.; Fujita, T.; Chen, M. W.; Erlebancher, J. Oxygen Reduction in Nanoporous Metal−Ionic Liquid Composite Electrocatalysts. *Nat. Mater.* **2010**, *9*, 904−907.
(2) Shao, M. H.; Sasaki, K.; Adzic, R. R. Pd-Fe Nanoparticles as Electrocatalysts for Oxygen Reduction. *J. Am. Chem. Soc.* **2006**, *128*, 3526−3527.
(3) Jeon, M. K.; Lee, C. H.; Park, G. I.; Kang, K. H. Combinatorial Search for Oxygen Reduction Reaction Electrocatalysts: A Review. *J. Power Sources* **2012**, *216*, 400−408.
(4) Zhang, L.; Wang, L.; Holt, C. M. B.; Zahiri, B.; Li, Z.; Malek, K.; Navessin, T.; Eikerling, M. H.; Mitlin, D. Highly Corrosion Resistant Platinum-Niobium Oxide-Carbon Nanotube Electrodes for the Oxygen Reduction in PEM Fuel Cells. *Energy Environ. Sci.* **2012**, *5*, 6156−6172.
(5) He, F. A.; Fan, J. T.; Ma, D.; Zhang, L. M.; Leung, C.; Chan, H. L. The Attachment of Fe_3O_4 Nanoparticles to Graphene Oxide by Covalent Bonding. *Carbon* **2010**, *48*, 3139−3144.
(6) Jiang, S.; Zhu, C. Z.; Dong, S. J. Cobalt and Nitrogen-Cofunctionalized Graphene as a Durable Non-Precious Metal Catalyst with Enhanced ORR Activity. *J. Mater. Chem. A* **2013**, *1*, 3593−3599.
(7) Liang, Y. Y.; Li, Y. G.; Wang, H. L.; Zhou, J. G.; Wang, J.; Regier, T.; Dai, H. J. Co_3O_4 Nanocrystals on Graphene As a Synergistic Catalyst for Oxygen Reduction Reaction. *Nat. Mater.* **2011**, *10*, 780−786.
(8) Musameh, M.; Lawrence, N. S.; Wang, J. Electrochemical Activation of Carbon Nanotubes. *Electrochem. Commun.* **2005**, *7*, 14−18.
(9) Xiao, J.; Mei, D. H.; Li, X. L.; Xu, W.; Wang, D. Y.; Graff, G. L.; Bennett, W. D.; Nie, Z. M.; Saraf, L. V.; Aksay, I. A.; Liu, J.; Zhang, J.-G. Hierarchically Porous Graphene as a Lithium−Air Battery Electrode. *Nano Lett.* **2011**, *11*, 5071−5078.
(10) Yan, J.; Liu, J. P.; Fan, Z. J.; Wei, T.; Zhang, L. J. High-Performance Supercapacitor Electrodes Based on Highly Corrugated Graphene Sheets. *Carbon* **2012**, *50*, 2179−2188.
(11) Liu, R. L.; Wu, D. Q.; Feng, X. L.; Müllen, K. Nitrogen-Doped Ordered Mesoporous Graphitic Arrays with High Electrocatalytic Activity for Oxygen Reduction. *Angew. Chem., Int. Ed.* **2010**, *122*, 2619−2623.
(12) Wen, Z. H.; Liu, J.; Li, J. H. Core/Shell Pt/C Nanoparticles Embedded in Mesoporous Carbon as a Methanol-Tolerant Cathode Catalyst in Direct Methanol Fuel Cells. *Adv. Mater.* **2008**, *20*, 743−747.
(13) Zheng, Y.; Liu, J.; Liang, J.; Jaroniecc, M.; Qiao, S. Z. Graphitic Carbon Nitride Materials: Controllable Synthesis and Applications in Fuel Cells and Photocatalysis. *Energy Environ. Sci.* **2012**, *5*, 6717−6731.
(14) Lyth, S. M.; Nabae, Y.; Moriya, S.; Kuroki, S.; Kakimoto, M.; Ozaki, J.; Miyata, S. Carbon Nitride as a Nonprecious Catalyst for Electrochemical Oxygen Reduction. *J. Phys. Chem. C* **2009**, *113*, 20148−20151.
(15) Kwon, K.; Sa, Y. J.; Cheon, J. Y.; Joo, S. H. Ordered Mesoporous Carbon Nitrides with Graphitic Frameworks as Metal-Free, Highly Durable, Methanol-Tolerant Oxygen Reduction Catalysts in an Acidic Medium. *Langmuir* **2012**, *28*, 991−996.
(16) Wang, Y.; Zhang, J. S.; Wang, X. C.; Antonietti, M.; Li, H. R. Boron- and Fluorine-Containing Mesoporous Carbon Nitride Polymers: Metal-Free Catalysts for Cyclohexane Oxidation. *Angew. Chem., Int. Ed.* **2010**, *49*, 3356−3359.
(17) Liu, G.; Niu, P.; Sun, C. H.; Smith, S. C.; Chen, Z. G.; Lu, G. Q.; Cheng, H. M. Unique Electronic Structure Induced High Photoreactivity of Sulfur-Doped Graphitic C_3N_4. *J. Am. Chem. Soc.* **2010**, *132*, 11642−11648.
(18) Yang, W.; Fellinger, T.-P.; Antonietti, M. Efficient Metal-Free Oxygen Reduction in Alkaline Medium on High-Surface-Area Mesoporous Nitrogen-Doped Carbons Made from Ionic Liquids and Nucleobases. *J. Am. Chem. Soc.* **2011**, *133*, 206−209.
(19) Rao, C. V.; Cabrera, C. R.; Ishikawa, Y. In Search of the Active Site in Nitrogen-Doped Carbon Nanotube Electrodes for the Oxygen Reduction Reaction. *J. Phys. Chem. Lett.* **2010**, *1*, 2622−2627.
(20) Wang, Y.; Shao, Y. Y.; Matson, D. W.; Li, J. H.; Lin, Y. H. Nitrogen-Doped Graphene and Its Application in Electrochemical Biosensing. *ACS Nano* **2010**, *4*, 1790−1798.
(21) Choi, C. H.; Chung, M. W.; Kwon, H. C.; Parka, S. H.; Woo, S. I. B, N- and P, N-Doped Graphene as Highly Active Catalysts for Oxygen Reduction Reactions in Acidic Media. *J. Mater. Chem. A* **2013**, *1*, 3694−3699.
(22) Zhao, Y.; Yang, L. J.; Chen, S.; Wang, X. Z.; Ma, Y. W.; Wu, Q.; Jiang, Y. F.; Qian, W. J.; Hu, Z. Can Boron and Nitrogen Co-doping Improve Oxygen Reduction Reaction Activity of Carbon Nanotubes? *J. Am. Chem. Soc.* **2013**, *135*, 1201−1204.
(23) Liu, Z.; Nie, H. G.; Yang, Z.; Zhang, J.; Jin, Z. P.; Lu, Y. Q.; Xiao, Z. B.; Huang, S. M. Sulfur-Nitrogen Co-Doped Three-Dimensional Carbon Foams with Hierarchical Pore Structures as Efficient Metal-Free Electrocatalysts for Oxygen Reduction Reactions. *Nanoscale* **2013**, *5*, 3283−3288.
(24) Liu, Y. M.; Chen, S.; Quan, X.; Yu, H. T.; Zhao, H. M.; Zhang, Y. B.; Chen, G. H. Boron and Nitrogen Codoped Nanodiamond as an Efficient Metal-Free Catalyst for Oxygen Reduction Reaction. *J. Phys. Chem. C* **2013**, *117*, 14992−14998.
(25) Xu, J. X.; Zhao, Y.; Shen, C.; Guan, L. H. Sulfur- and Nitrogen-Doped, Ferrocene-Derived Mesoporous Carbons with Efficient Electrochemical Reduction of Oxygen. *ACS Appl. Mater. Interfaces* **2013**, *5*, 12594−12601.
(26) Yeh, T. F.; Syu, J. M.; Cheng, C.; Chang, T. H.; Teng, H. Graphite Oxide as a Photocatalyst for Hydrogen Production from Water. *Adv. Funct. Mater.* **2010**, *20*, 2255−2262.
(27) Dong, F.; Wu, L.; Sun, Y.; Fu, M.; Wu, Z.; Lee, S. C. Efficient Synthesis of Polymeric g-C_3N_4 Layered Materials as Novel Efficient Visible Light Driven Photocatalysts. *J. Mater. Chem.* **2011**, *21*, 15171−15174.
(28) Liu, Q.; Zhang, J. Y. Graphene Supported Co-g-C_3N_4 as a Novel Metal−Macrocyclic Electrocatalyst for the Oxygen Reduction Reaction in Fuel Cells. *Langmuir* **2013**, *29*, 3821−3828.
(29) Mao, S.; Yu, K. H.; Cui, S. M.; Bo, Z.; Lu, G. H.; Chen, J. H. A New Reducing Agent to Prepare Single-Layer, High-Quality Reduced Grapheme Oxide for Device Applications. *Nanoscale* **2011**, *3*, 2849−2853.
(30) Li, R.; Wei, Z. D.; Gou, X. L.; Xu, W. Phosphorus-Doped Graphene Nanosheets as Efficient Metal-Free Oxygen Reduction Electrocatalysts. *RSC Adv.* **2013**, *3*, 9978−9984.
(31) Li, X. F.; Zhang, J.; Shen, L. H.; Ma, Y. M.; Lei, W. W.; Cui, Q. L.; Zou, G. T. Preparation and Characterization of Graphitic Carbon Nitride through Pyrolysis of Melamine. *Appl. Phys. A: Mater. Sci. Process.* **2009**, *94*, 387−392.
(32) Panchakarla, L. S.; Govindaraj, A.; Rao, C. N. R. Nitrogen- and Boron-Doped Double-Walled Carbon Nanotubes. *ACS Nano* **2007**, *1*, 494−500.
(33) Ozaki, J.; Kimura, N.; Anahara, T.; Oya, A. Preparation and Oxygen Reduction Activity of BN-Doped Carbons. *Carbon* **2007**, *45*, 1847−1853.
(34) Sheng, Z. H.; Gao, H. L.; Bao, W. J.; Wang, F. B.; Xia, X. H. Synthesis of Boron Doped Graphene for Oxygen Reduction Reaction in Fuel Cells. *J. Mater. Chem.* **2012**, *22*, 390−395.
(35) Han, J. C.; Liu, A. P.; Zhu, J. Q.; Tan, M. L.; Wu, H. P. Effect of Phosphorus Content on Structural Properties of Phosphorus Incorporated Tetrahedral Amorphous Carbon Films. *Appl. Phys. A: Mater. Sci. Process.* **2007**, *88*, 341−345.
(36) Yang, D. S.; Bhattacharjya, D.; Inamdar, S.; Park, J.; Yu, J. S. Phosphorus-Doped Ordered Mesoporous Carbons with Different Lengths as Efficient Metal-Free Electrocatalysts for Oxygen Reduction Reaction in Alkaline Media. *J. Am. Chem. Soc.* **2012**, *134*, 16127−16130.
(37) Wang, S. Y.; Iyyamperumal, E.; Roy, A.; Xue, Y. H.; Yu, D. S.; Dai, L. M. Vertically Aligned BCN Nanotubes as Efficient Metal-Free Electrocatalysts for the Oxygen Reduction Reaction: A Synergetic

Effect by Co-Doping with Boron and Nitrogen. *Angew. Chem., Int. Ed.* **2011**, *50*, 11756−11760.
(38) Paraknowitsch, J. P.; Thomas, A. Doping Carbons beyond Nitrogen: an Overview of Advanced Heteroatom Doped Carbons with Boron, Sulphur and Phosphorus for Energy Applications. *Energy Environ. Sci.* **2013**, *6*, 2839−2855.
(39) Zheng, Y.; Jiao, Y.; Ge, L.; Jaroniec, M.; Qiao, S. Z. Two-Step Boron and Nitrogen Doping in Graphene for Enhanced Synergistic Catalysis. *Angew. Chem., Int. Ed.* **2013**, *125*, 3192−3198.
(40) Yu, D. S.; Xue, Y. H.; Dai, L. M. Vertically Aligned Carbon Nanotube Arrays Co-doped with Phosphorus and Nitrogen as Efficient Metal-Free Electrocatalysts for Oxygen Reduction. *J. Phys. Chem. Lett.* **2012**, *3*, 2863−2870.
(41) Wang, D. W.; Su, D. S. Heterogeneous Nanocarbon Materials for Oxygen Reduction Reaction. *Energy Environ. Sci.* **2014**, *7*, 576−591.
(42) Choi, C. H.; Park, S. H.; Woo, S. I. Binary and Ternary Doping of Nitrogen, Boron, and Phosphorus into Carbon for Enhancing Electrochemical Oxygen Reduction Activity. *ACS Nano* **2012**, *6*, 7084−7091.
(43) Cruz-Silva, E.; Lopez-Urıas, F.; Munoz-Sandoval, E.; Sumpter, B. G.; Terrones, H.; Charlier, J.-C.; Meunier, V.; Terrones, M. Electronic Transport and Mechanical Properties of Phosphorus- and Phosphorus-Nitrogen-Doped Carbon Nanotubes. *ACS Nano* **2009**, *3*, 1913−1921.
(44) Liang, J.; Jiao, Y.; Jaroniec, M.; Qiao, S. Z. Sulfur and Nitrogen Dual-Doped Mesoporous Graphene Electrocatalyst for Oxygen Reduction with Synergistically Enhanced Performance. *Angew. Chem., Int. Ed.* **2012**, *51*, 11496−11500.